MNRAS **000**, 1–9 (2018) Preprint 20 June 2018 Compiled using MNRAS LATEX style file v3.0

Substructures in Minor Mergers' Tidal Streams

D. A. Noreña[1]★, J. C. Muñoz-Cuartas[1]†, L. F. Quiroga[1] and N. Libeskind[2]
[1]*FACom - Instituto de Física, FCEN, Universidad de Antioquia (UdeA), Calle 70 No. 52-21, Medellín, Colombia.*
[2]*Leibniz-Institut für Astrophysik Potsdam (AIP), An der Sternwarte 16, D-14482 Potsdam, Germany.*

Accepted XXX. Received YYY; in original form ZZZ

ABSTRACT
In this work, we explore the idea that stellar and/or gaseous substructures like stellar clusters could be formed from the tidal stream material produced in galactic minor mergers. We use two sets of N-body simulations of satellite galaxies interacting with a larger host galaxy. The first set used satellites devoid of gas while the second set used satellites with a gaseous component including star-formation and supernova feedback. We estimated the spatial distribution of mass to identify overdensity regions in which a substructure could be formed. As a first conclusion, we found that without gas, no substructure formed as none of the overdensities show a definite morphology or dynamical stability over time. Conversely, including gas resulted in a remarkably different behavior, several clumps appear and they proved to be real physical structures that remained for a considerable time ($\geq$ 1 Gyr). Furthermore, the study of the orbital structure, ages and masses of the overdensities lead us to conclude that substructures (star clusters or high-velocity clouds) can be formed in tidal streams of gas-rich satellites. Also, evidence was found favoring the presence of dark matter in the substructures after the formation process, adding to the discussion about the formation of star clusters and providing an observational mechanism to verify the reliability of the model.

Key words: galaxies: formation – galaxies: interactions – galaxies: evolution – star clusters: general – *(galaxies:)* intergalactic medium – *(Galaxy:)* globular clusters: general – *(Galaxy:)* open clusters and associations: general – galaxies: star clusters: general – methods: numerical

1 INTRODUCTION

The galactic halo is plenty of astrophysical systems evolving under the interactions with the different galactic components. These substructures have diverse nature, dynamics and origins and together constitute the building blocks of the ongoing galaxy formation. Among others, there are stellar subsystems as the open and globular clusters (Binney & Tremaine 2008), pure gaseous ones as high velocity clouds (HVC) (Wakker & van Woerden 1997) and combined gaseous and stellar systems such as tidal streams and satellite galaxies (Ibata et al. 2001).

Open and globular clusters are segregated by several characteristics. Open clusters are considered as more young, metal rich than their globular counterparts, without discounting in addition that the open ones are associated spatially with the galactic disc while globular are distributed spherically all around the halo. The cluster segregation can only signify that their formation processes are equally diverse, in one hand, the formation of open clusters is considered well understood as the collapse and fragmentation of the disc molecular clouds (Elmegreen & Efremov 1997). The case of globular clusters exhibits a greater degree of complexity because actually there are two subpopulations of them, the widely known old, metal poor (MPGC) extended across the halo, and the younger, metal rich (MRGC) and disc associated ones (Carroll & Ostlie 2006). In addition, there are several cases that do not fit very well in the two previous subpopulations as the globular cluster ω-Centauri mainly due to its unusual size and metallicity dispersion (Harris 1999). This variety suggests that even only for the globular kind of star clusters there are diverse formation mechanisms.
Different models have been proposed to explain possible formation mechanisms for the two subpopulations of globular clusters in The Galaxy. For the Old MPGC subpopulation the widely accepted hypothesis is that they come from primordial density fluctuations in the density field at very high redshift, when the universe expanded and cooled to a temperature of about 4000K and the baryonic density was ap-

★ Email : david.norena@udea.edu.co
† Email : juan.munozc@udea.edu.co

proximately 10^4 atoms cm^{-3}. Under this conditions, the only density fluctuations that can grow with time has wavelength in excess of the critical Jeans length of about 5 pc (Peebles & Dicke 1968).

For the young MRGC subpopulation, several models have been proposed but it appears that there is not a single mechanism that can form all existing MRGC in a given galaxy. One of the main models suggests that a significant fraction of the metal-rich subpopulation may have originated in interacting galaxies, both minor and major mergers (Ashman & Zepf 1992). Major mergers cause several starburst episodes in the gaseous component of each galaxy, and globular clusters can be formed in regions with high gas density (Li et al. 2004). Minor mergers may also contribute to the young population with clusters formed within the small satellite galaxy from the interaction with the larger galaxy (Zepf & Ashman 1993). Also, the globular cluster system of the minor galaxy would eventually be accreted by the largest galaxy, also contributing to the MPGCs subpopulation (Forbes & Bridges 2010). The minor merger scenario can be seen in the Magellanic Clouds, where there is observational evidence of ongoing cluster formation and an ancient cluster system bound to the clouds (Harris 1998). It was further suggested that a satellite galaxy can generate globular clusters by tidal stripping caused by the larger galaxy, along the orbital motion of the satellite the tidal forces will despoil the stars of the outermost layers of the satellite, finally leaving the core of the satellite galaxy, the new globular cluster (Bekki & Chiba 2002).

Moreover, recently observational evidence that suggests that several (if not all) GCs contain various stellar populations has come to light. For example, many GC stars have the same amount of Fe (and other heavy elements) inside a specific radius, but a wide variation in light elemental abundance (Li-Ai) on a star-to-star basis (Conroy et al. 2011). Norris & Kannapan (2011) showed that some ultra-compact dwarf galaxies have color magnitude diagrams indistinguishable from GCs and the nuclei of dwarf galaxies. Bekki & Freeman (2003) found that the multiple stellar populations of ω-Cen can be explained in terms of a nucleated dwarf galaxy scenario: the tidal field of the host galaxy induces gas inflow towards the center of the cluster progenitor, triggering multiple star bursts that lead to chemical enrichment. Other GC candidates that are thought to have formed in ostensibly dark matter potentials deep enough to retain self-enriched Fe produced by supernovae Ia explosions include M22, NGC 1851 and Andromeda's G1. The evidence showing chemical complexity of the cluster stellar populations suggest that the classical picture of all GC's belonging to a single monolithic populations should be reevaluated.

Similarly, HVCs appear to be the result of two possible mechanisms: one is the return to the disc of gas and dust expelled via supernovae events and the other is the falling to the disc of gas and dust material from a stripped away subsystem, such as a globular clusters or a satellite galaxies (Wakker & van Woerden 1997).

A combination of both processes is necessary to explain the current distribution of high and intermediate velocity clouds. For example, from hydrodynamical simulations it is concluded that most massive HVC such as the well known Complex C were originated from ejection of material from the Milky Way's disc (Fraternali et al. 2015); but the velocity dispersion, the metallicity, sizes and masses of the smallest clouds are consistent with an extragalactic origin (Blitz et al. 1999; Binney et al. 2009).

As a result of the tidal disruption of the Galaxy subsystems, the called tidal streams are originated. They are composed in most cases by stars and gas, having been observed pure gaseous streams like the Magellanic Stream (Belokurov et al. 2006). Remarkably, all the streams observed in the Milky Way galaxy have overdensities within them, this is, regions with a number of stars greater than the rest of the structure (Küpper et al. 2012).

The overdensities evolve in the galactic potential as well, undergoing different processes that could eventually transform them into self gravitating systems resembling the clusters and the gas clouds. The main purpose of this work is to determine through $N-$body simulations of galaxy minor mergers if the overdensities in the the tidal streams could really meet the conditions to be considered self-gravitating substructures. In a future work, we will investigate under what conditions the evolution of such substructures could lead to the formation of real astrophysical systems such as globular clusters and high velocity clouds.

This paper is organized as follows: In Section 2 we describe the whole setup of the $N-$body simulations, from the determination of the satellite galaxy initial position to the structure of the host galaxy passing through the astrophysical characteristics of the satellite. In Section 3 we describe the analysis performed to the simulations outputs in order to search and characterize the overdensities. In Section 4 we present our results to finally discuss them and present the conclusions in Section 5.

2 NUMERICAL PROCEDURES

The numerical setup of the $N-$ body simulations comprises two stages. In the first instance the galaxies were generated isolated, in this case, we generate a host disc galaxy with its dark matter halo and a spheroidal satellite galaxy, with and without gas content. Then, we configure the initial positions of the interacting galaxies and finally we describe the simulations performed. In the following sections we describe in detail each procedure.

2.1 Initial conditions

2.1.1 Isolated Galaxies

To study the potential formation of substructures from tidal streams we use numerical $N-$body simulations of minor mergers. The host galaxy in this model consists of a disk galaxy composed by a stellar disk and a dark matter halo. The central spheroid is not included.

Initial conditions were computed using moments of the collisionless Boltzmann equation (Hernquist 1993; Springel & White 1999; Springel et al. 2004). Host dark matter halo follows a Hernquist density profile with scale length parameter adjusted to fit the shape of the NFW density profile as done in (Springel et al. 2004).

The satellite galaxy is modeled as an spherical system with a Hernquist density profile.

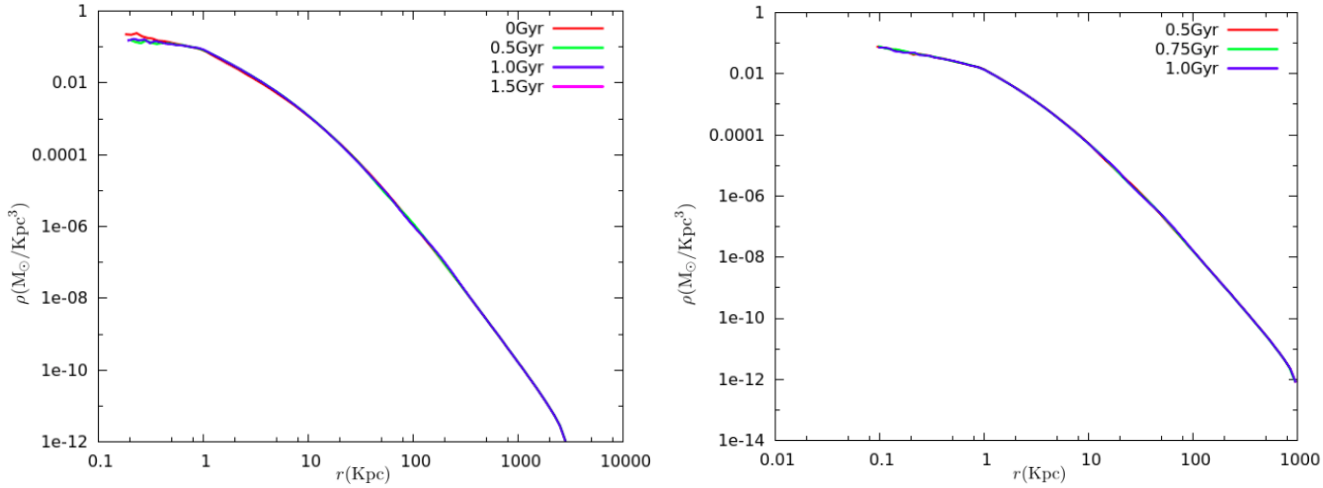

Figure 1. Convergence of the density profiles of the host(left) and satellite's(right) dark matter halos under numerical relaxation. The galaxies where evolved isolated, the host by 1.5 Gyr and the satellite by 1 Gyr.

Masses for the galaxies are taken from the CLUES simulations (Gottloeber et al. 2010; Forero-Romero et al. 2011). The mass of the dark matter halo hosting the disk galaxy is $7.9 \times 10^{11} h^{-1} \mathrm{M}_\odot$, while the satellite has a total mass of $3.2 \times 10^{10} h^{-1} \mathrm{M}_\odot$. Since it is not reasonable to simulate the formation of globular clusters observed today using properties of current host galaxies, the masses and properties of these two progenitor galaxies are related to the properties of the Milky Way galaxy and one of its satellites at $z = 2$ as observed from the constrained simulations made by CLUES. Galaxy disk structure (disk scale length, etc) is modeled using (Mo et al. 1998) prescription.

The host galaxy has a stellar disk with a mass of $3.3 \times 10^{9} h^{-1} \mathrm{M}_\odot$where we have used (Moster et al. 2010) to estimate the total stellar mass for the given dark matter halo at $z = 2$ and assumed that all the stellar mass is deposited in the disk. Since we are not interested in the evolution of the gas in the disk of the host galaxy we do not include a gaseous component into this galaxy.

The satellite galaxy is composed of collisionless components (dark matter/stars) and gas. Initially, the gas follows a density profile similar to the profile of the dark matter halo but in hydrostatic equilibrium. Hydrostatic equilibrium is guaranteed through gas temperature which is computed as (Mastropietro et al. 2005)

$$T(r) = \frac{m_p}{k_B \rho_g(r)} \int_r^\infty \rho(r) \frac{GM(r)}{r^2} \mathrm{d}r, \tag{1}$$

where m_p is the proton mass, k_B is the Boltzmann constant and $\rho_g(r)$ is the gas mas density. In order to provide a favorable scenario for the formation of clusters from the material deposited in the stream, the total gas mass in the satellite has been chosen to be $\sim 16\%$ of its total mass, providing the scenario for a *wet merger*.

All galaxies are allowed to be relaxed after the generation of initial conditions in order to allow numerical relaxation of the initial conditions. Figure 1 shows the convergence of the profiles from the initial conditions to the final relaxed density profile. Note that the mass distribution only changes in their very inner region and after the first 1 Gyr the profile is relaxed. Also, the satellite galaxy reaches relaxation basically very close from the beginning.

It is important to ensure that there are not induced numerical artificial evolution on the density distribution of the galaxies, so we can ensure that any change in the mass distribution of the system is due to the dynamics of the merger and is not spurious numerical noise.

2.1.2 Merger configuration

The initial position of the host galaxy was chosen as the origin of coordinates and the initial position of the satellite was chosen according to the procedure described in Wetzel (2011).

The initial position $\mathbf{r}_0$ and velocity $\mathbf{v}_0$ of the satellite galaxy were established by determining the most probable orbital parameters that the subhalos infalling a host halo will have. The circularity η and the pericenter r_p depend on the host halo mass M_{host} and redshift z and are distributed at the moment of their passage through the host's virial radius according to the distribution functions showed in figures 2 and 3 for our host halo at different redshifts. In both figures, the average values of the circularity and the pericentre at $z = 2$ are highlighted with a small vertical green line.

From CLUES simulations, the mass of the host is $M_{\mathrm{host}} = 4.6 \times 10^{11} \mathrm{M}_\odot$ at $z = 2$. Then, we determine the distributions of pericentres and circularities at infall for our simulations (Wetzel 2011). Orbit circularity has a nearly constant small rate of decrease with redshift while pericenter distance exhibits a decrease in its average values with z. In particular, at $z = 2$ we obtain an average pericentric distance of $0.27 R_{\mathrm{vir}}$, with R_{vir} the virial radius of the host halo. For this halo $R_{\mathrm{vir}} \approx r_{200} = 63.29$ Kpc. The average circularity at $z = 2$ is 0.54. With this two values we calculate the eccentricity e and apocentric distance r_a using the two body approximation as

$$e = \sqrt{1 - \eta^2}, \tag{2}$$

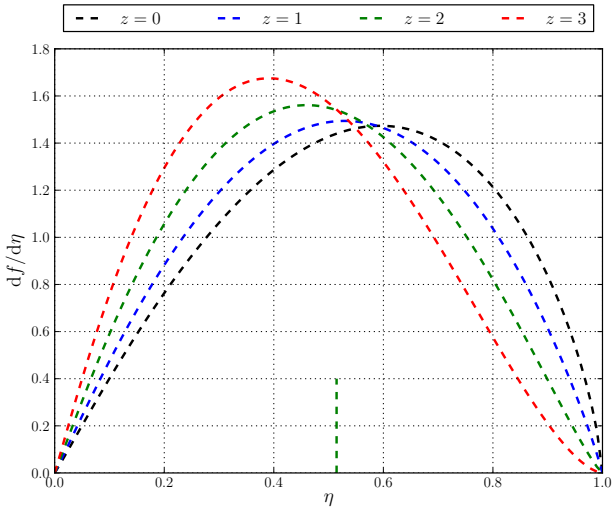

Figure 2. Circularity distribution for the infalling satellites at different redshifts. The small vertical line indicates the average circularity at $z = 2$.

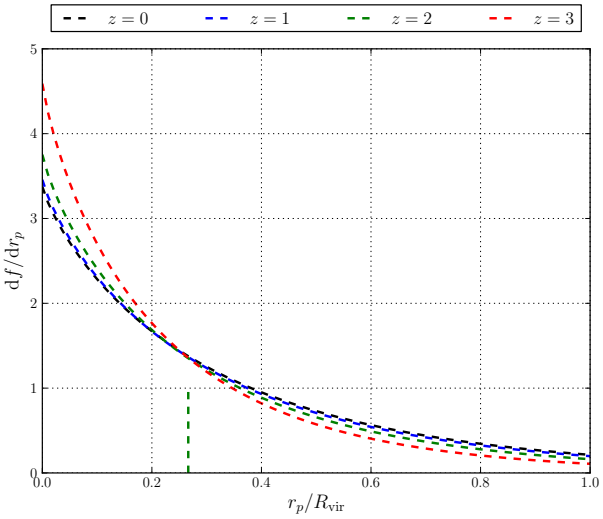

Figure 3. Pericentre distribution for the infalling satellites, redshift dependence is explicitly noted. The small vertical line indicates the avarage pericentric distance value at $z = 2$.

$$r_a = \left(\frac{1+e}{1-e}\right) r_p. \tag{3}$$

For our system, the numerical values were found to be $e = 0.84$ and $r_a = 198.34$ Kpc. Finally, making use of the *vis-viva* equation, the velocity at apogalacticon is simply

$$v_a = \sqrt{2\frac{GM}{r_a}(1-e)}, \tag{4}$$

which turns to be 34.9 Km/s for our infalling satellite. Based on the satellite parameters given in the previous paragraph, the merger was disposed in five different configurations. Its main differences are their location relative to the disc plane and its orbital motion direction relative to the disc rotation. The configuration parameters are shown in table 1 and a schematic illustration of all of them are represented in figure 4.

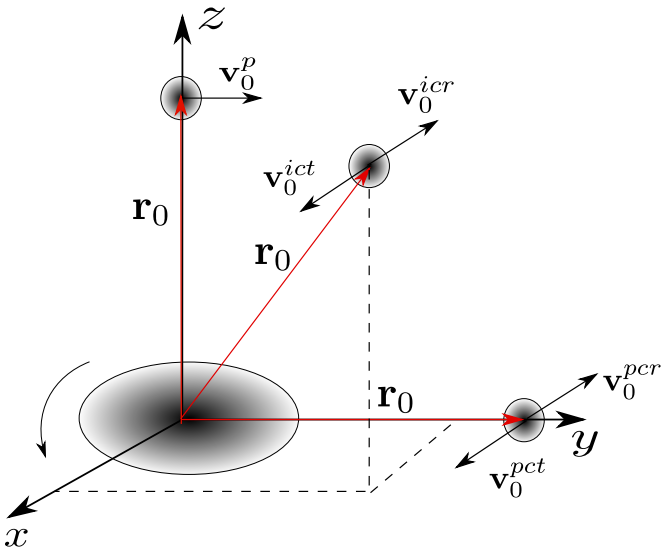

Figure 4. Schematic representation of the initial orbital configurations for the original five simulations. The host disc is rotating counterclockwise in the $xy-$plane. $\mathbf{r}_0$ and $\mathbf{v}_0$ are the initials position and velocity in each case. See table 1.

2.2 Simulations

The $N-$body simulations of this work were performed using the open source code GADGET2 (Springel 2005) which is able to evolve either collisional and collisionless particles. The code uses SPH to follow the evolution of the gas inside the galaxy. Star formation is modeled as shown in (Springel & Hernquist 2002). As is well known, SPH suffers from fragmentation instabilities that lead small gas clumps to cluster forming a set of non-physical structures (Bate & Burkert 1997; Torrey et al. 2013). Since what we are looking for in our simulations is exactly fluctuations in the mass distribution we need to make sure that what we find as candidates are not just spurious numerical fragments formed due to the SPH instability. In order to avoid this, we ran the same set of initial conditions for several different particle resolutions. Increasing the resolution of the simulations allow us to verify that what we find as globular cluster candidates are true candidates and not numerical artifacts.

We design two sets of experiments to explore the formation of substructures in the tidal tails of the satellite galaxy. The first consists in pure collisionless systems, or in other words, does not include gas. The main purpose of these first experiment was verify if the dark matter alone could cluster and form bound systems without the influence of gas. This set was nominated as DMO (Dark Matter Only), specifically DMO1 and DMO2 whose only difference is the satellite number of particles as is reflected in Table 2 where are shown

Name	Nomenclature	$\mathbf{r}_0$ (Kpc)	$\mathbf{v}_0$(Km/s)
Perpendicular	*p*	(0,0,198.34)	(0,34.9,0)
Planar Corrotating	*pcr*	(0,198.34,0)	(-34.9,0,0)
Planar Contrarotating	*pct*	(0,198.34,0)	(34.9,0,0)
Inclined Corrotating	*icr*	(99.6,99.6,140.25)	(-24.67,24.67,0)
Inclined Contrarotating	*ict*	(99.6,99.6,140.25)	(24.67,-24.67,0)

Table 1. Specifications of the satellite's initial orbital configurations chosen for each simulation. For a schematic view of each configuration, see figure 4.

Name	Component	Mass	N_p	m_p
DMO2	Satellite	3.2×10^{10}	2×10^{5}	1.6×10^{5}
	Disk	3.3×10^{9}	5.6×10^{4}	6.4×10^{4}
	Halo	7.9×10^{11}	7.3×10^{5}	1.1×10^{6}

Table 2. Collisionless simulations. N_p and m_p are the number of particles and mass per particle respectively.

Name	Component	Mass	N_p	m_p
GAS1	Satellite	2.5×10^{10}	4×10^{4}	6.2×10^{4}
	Gas	5×10^{9}	2×10^{4}	2.5×10^{4}
	Disk	3.3×10^{9}	5.6×10^{4}	6×10^{4}
	Halo	7.9×10^{11}	7.3×10^{5}	1.1×10^{6}
GAS2	Satellite	2.5×10^{10}	8×10^{5}	3.1×10^{4}
	Gas	5×10^{9}	4×10^{5}	1.25×10^{3}
	Disk	3.3×10^{9}	5.6×10^{4}	6.4×10^{4}
	Halo	7.9×10^{11}	7.3×10^{5}	1.1×10^{6}
GAS3	Satellite	2.5×10^{10}	3×10^{6}	8.3×10^{3}
	Gas	5×10^{9}	1×10^{6}	5×10^{3}
	Disk	3.3×10^{9}	5.6×10^{4}	6.4×10^{4}
	Halo	7.9×10^{11}	1×10^{7}	7.9×10^{4}

Table 3. Collisional simulations. N_p and m_p are the number of particles and mass per particle respectively.

the masses, number of particles and mass per particle of each component.

The second set of simulations included the satellite gas and were designated with the nomenclature GAS. The difference among them is the increasing number of particles, being GAS3 the one with the highest resolution. Table 3 summarizes the resolution specifications of the GAS experiment.

As it can be seen in table 3 the SPH particle mass is of the order of 5×10^3 $h^{-1}\mathrm{M}_\odot$. If we assume that typical mases for globular cluster candidates are of the order of 10^5 to 10^7 $h^{-1}\mathrm{M}_\odot$in this simulation we could resolve globular cluster candidates with 20 to 2000 gas particles. We have run our simulations during a time interval of the order of 7 Gyr, enough to study the evolution of the satellite remnants as it would be observed in present time.

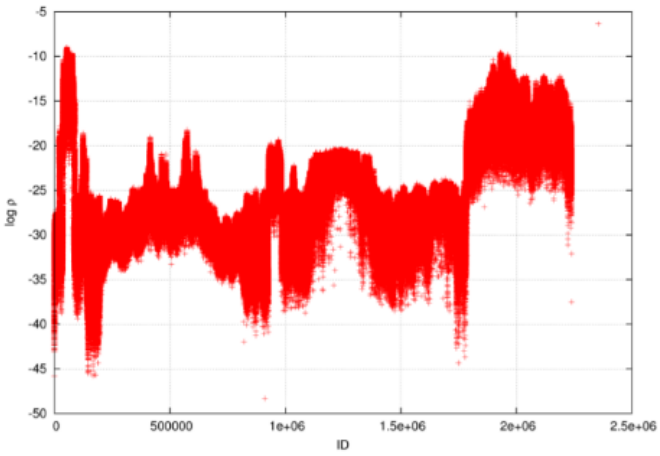

Figure 5. Density values for the particles in GAS2 $p-$simulation against the identification particle number. This plot correspond to the snapshot at 3.75 Gyr after simulation start. Density units are $10^{10}\mathrm{M}_\odot/\mathrm{Kpc}^3$

3 ANALYSIS

3.1 Density Estimation

Overdensities are by definition regions with spatial mass density greater than its surroundings. Hence, the best way to identify them is by estimating mass density in the body of the tidal streams. High density regions will be the best candidates to form autogravitating substructures. We implement the EnBiD (Entropy Based Binary Decomposition) algorithm to calculate the density distribution in real and phase spaces (Sharma & Steinmetz 2006).

The EnBiD algorithm is sensitive to the spatial anisotropies of the mass distribution by the implementation of the anisotropic smoothing tensor. In this way, the density underestimation is prevented due to the capacity of compute particles along certain directions and not only spherically around the point as the isotropic common kernels do. Figure 5 shows the estimated density for the total number of particles in one of the GAS simulations where we have we have the density of gas particles accommodated in the interval 0 to 254835 at the *x* axis, halo dark matter particles in the interval 254836 to 986212, disk particles ranged from 986213 to 1042222, satellite particles go from 1042223 to 1842222 and new stars formed in the gas comprising the interval between 1842223 to 2222800.

3.2 Substructures Candidates Identification

Once the densities of the particles have been calculated, we aimed to identify the overdensities in the field of the stream in order to manage them as possible candidates. We start by construct density maps in real space from estimation performed before. These maps highlight the overdensities above the underlying distribution of particles as is shown in figures 7 and 8. Then, the identification is carried out by the following series of steps:

- First the candidates are identified by performing a selection of particles through a phase space density threshold ρ_{th}. Particles with phase-space densities below the density threshold are definitely ruled out as potentially belonging to some candidate clump. The value of ρ_{th} was chosen examining the values of the density of the simulation using, for instance, a plot of the type of figure 5 in which we clearly distinguish between particles of high and low density.
- With the candidates identified, for each one of them, we determine the center of the distribution of particles in a particular snapshot of the simulation.
- Then, gas particles that are within a sphere of a reasonable radius R_0, centered in the center determined in the previous step were selected to track the candidate along the simulation.
- With the identification number of each particle in the candidate, we track the position and velocities of that particles in the snapshots preceding and following the one in which the identification was made. In this point, we look for particles of any kind that lie within a sphere or radius R_{th} that time, including dark matter particles from the host and the satellite haloes, disk particles or new stars born during the interaction.
- For every snapshot, we compute the properties of the clump in order to compare the evolution of the visually identified gas clouds with an astrophysical observed system.

3.3 Resolution Study Against Artificial Fragmentation

The numerical scheme used to simulate the hydrodynamics of the gas could impact the formation of clumps within the molecular clouds in an artificial way. The resolution of a SPH simulation involving gravity is therefore a critical quantity in order to obtain realistic results from physical process rather than artificially induced mechanisms by numerical fluctuations.

For SPH particles, the smoothing lengths h are constrained to contain approximately a number of particles $N_{\rm ngb}$ in a sphere of radius h, since the gravitational softening is set equal to h, the mass contained in the sphere can not be roughly equal to the local Jeans mass, otherwise the collapse is inhibited by the softening of the gravitational forces.

Thus, the called *minimum resolvable mass*, $M_{\rm res}$ must always be less than the local Jeans mass M_J given by

$$M_J = \left(\frac{3}{4\pi\rho}\right)^{1/2} \left(\frac{5k_BT}{\mu m_H G}\right)^{3/2}, \quad (5)$$

where ρ is the density of the gas at temperature T, k_B is the Boltzmann constant, m_H is the mass of the hydrogen atom

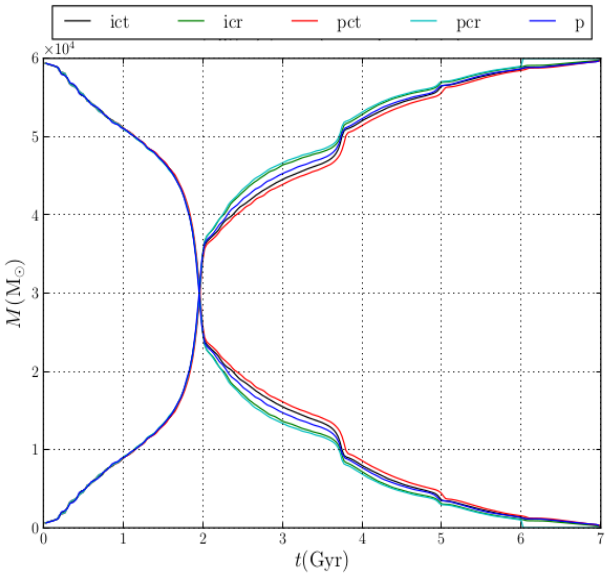

Figure 6. Mass striped out from the satellite galaxy as a function of simulation time represented by the descending curves for each orbital configuration. The mass gained by the stream for each orbital configuration are the ascending ones.

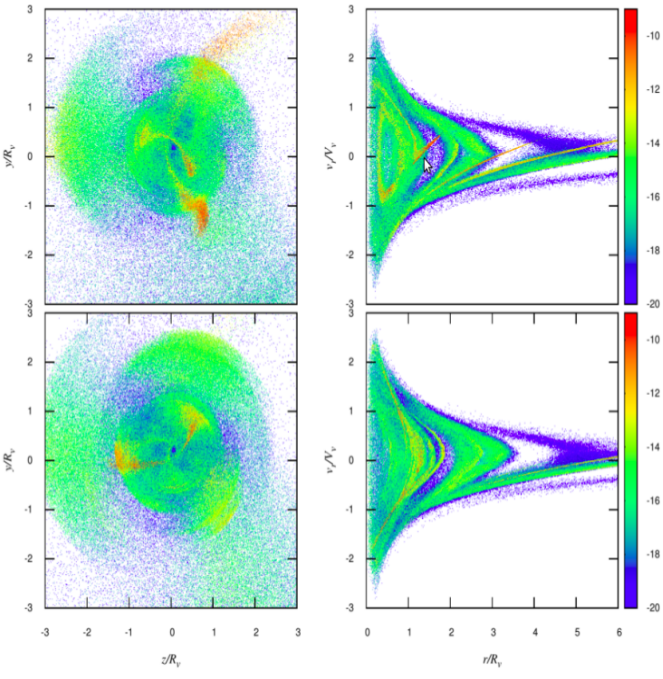

Figure 7. *Left Panel:* Real space projection on the $z-y$ mapped with density for DMO2 simulation. *Right Panel:* Phase space projection on the $r-v_r$ plane with same density color mapping. The density contrast is specially high in the tidal sparks, but still do not exhibit the morphology of globular clusters. Upper panels correspond to a time of 6.00 Gyr while bottom panels are at 7.00 Gyr.

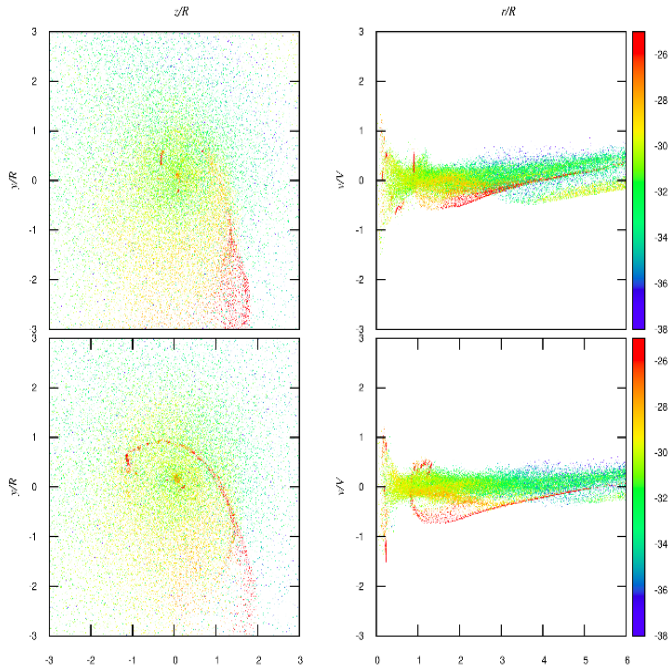

Figure 8. *Left Panel:* Real space projection on the $z-y$ mapped with density. *Right Panel:* Phase space projection on the $r-v_r$ plane with same density color mapping. R and V are the virial radius and velocity respectively. This corresponds to a couple of snapshots of GAS2. Upper panels correspond to a time of 5.00 Gyr while bottom panels are at 6.25 Gyr. Density units are $10^{10}\mathrm{M}_{\odot}/\mathrm{Kpc}^3$. Color values correspond to $\log\rho$.

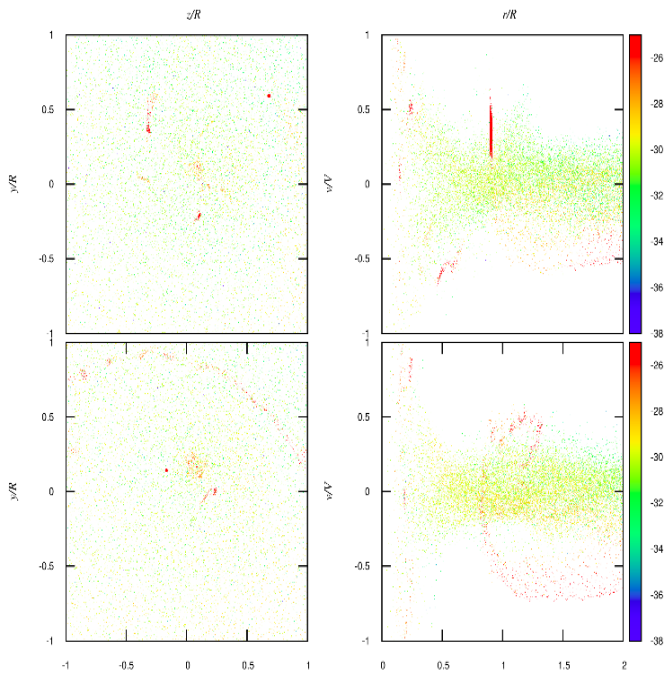

Figure 9. *Left Panel:* Real space projection on the $z-y$ mapped with density. *Right Panel:* Phase space projection on the $r-v_r$ plane with same density color mapping. This plot is exactly figure 7 but zooming to the internal region near the galactic disc for GAS2. ρ is in $10^{10}\mathrm{M}_{\odot}/\mathrm{Kpc}^3$. Upper panels correspond to a time of 5.00 Gyr while bottom panels are at 6.25 Gyr. Color values correspond to $\log\rho$.

and μ is the gas mean molecular weight (Draine 2011). Taking M_{res} as the mass of $2N_{\mathrm{ngb}}$ particles, it can be estimated as (Bate & Burkert 1997)

$$M_{\mathrm{res}} = M_{\mathrm{gas}}\left(\frac{2N_{\mathrm{ngb}}}{N_{\mathrm{gas}}}\right), \tag{6}$$

where M_{gas} and N_{gas} are the total mass and particle number of the gas. The previous expression explicitly shows that for a larger number of particles, the minimum resolvable mass decreases and the collapse and fragmentation will be less affected for the numerical implementation.
The condition (6) with $N_{\mathrm{ngb}} = 128$ is tested for the clumps in the satellite galaxy gas that we selected as substructures candidates with the previous recipe. The strategy adopted for the identification of the progenitors and the results obtained of such strategy are depicted in the next two sections.

4 RESULTS

In figure 6 we show the mass stripped out from the satellite galaxy as a function of simulation time. Each line in figure 6 represents the evolution of the mass stripped out from the satellite for each of the five orbital configurations presented in table 1. As it can be seen in the figure, the rate of mass loss is quite similar for every orbital configuration of the merger. For this reason, since we found no reason to prefer an orbit from any other, on the basis of the amount of mass stripped out of the satellite, we decided, without loss of generality, to run our high resolution simulations only for the configuration of the orbit perpendicular to the plane of the galaxy.

As it can be seen in the figure, there are breaks in the mass curve located at 2, 3.8 and 5 Gyr. These breaks are associated with the periastron passages during the merger. Clearly it is the first passage the one stripping the larger amount of mass out from the satellite. Most of the mass ejected during the first passage is gas that is heated up during the collision and should remain bounded to the host galaxy potentially forming overdensities that we are interested in to explore.

Figure 7 shows the projected particle distribution of the DMO2 simulation at two different time snapshots, $t = 6$ Gyr and $t = 7$ Gyr. The figure shows in color coded density the expected streams, and umbrella effects associated to the distribution of the merger remnant of a satellite interacting with a massive host galaxy. At the right, each figure shows the pseudo phase space diagrams, where it can be seen the disturbances in phase space associated to the structures of the streams and merger remnants. These overdensities were not stable with time, changing notably their morphologies.

Figure 8 represents the same projected particle distribution coded with density color than the former figure but for the GAS2 simulation but filtered by the density threshold. Unlike the case exposed in the previous paragraph, the overdensities survived for several orbital periods keeping their

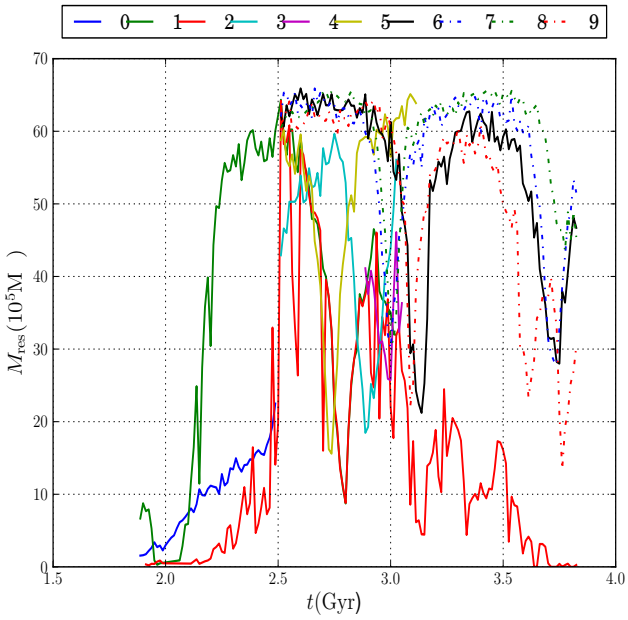

Figure 10. Minimun resolvable masses for the nine candidates in GAS3 (equation 6). The minimum mass remain much smaller than the candidates total mass, see figure 13.

structure for a significant lifetime fraction. Figure 9 is the inner region of figure 8 near the galactic disc.

GAS simulations are thus the ones with better results in the formation of streams substructures. Consequently, we targeted them to apply the *Substructures Candidates Identification* algorithm whose results are reflected in figure 12 where the galactic discs are included. The plots show the candidates identified at the same simulation time of 3 Gyr for comparison purposes. It is clearly evidenced that the higher resolution simulation, also the more realistic, has the greater number of substructures, which in turn, have the highest number of particles among all the simulations of this work. As is logical, we only study the properties of the substructures of GAS3.

For each identified substructure, we investigated several properties in order to characterize the nature of the substructures. In GAS3 were identified 10 overdensities labeled with integer numbers from 0 to 9 and for each one of them we start by determining their orbital evolution. Figure 11 (a) shows the yz projection of the center of mass orbits of the candidates. Figure 11 (b) is the representation of the candidates center of mass - center of the disc distance against time where the more notable aspect relies in the fact that the candidates persist among a significant amount of time.

Figure 13 shows the mass evolution of each candidate in GAS3. For all the candidates, the principal constituent is gas. The high picks of host dark matter content present in the candidates are circumstantial particles that are counted by the algorithm when the candidate traverses the central region of the dark halo where the density is sufficiently high to cause the miscounting of host dark particles as candidate particles. The masses founded in each candidate correspond to the masses measured for globular cluster and high-velocity clouds, both ranging from $10^3 M_\odot$ to a maximum of $10^6 M_\odot$ in average, although there are several cases of clusters with masses above of the $10^6 M_\odot$ value (Harris 1999; Wakker & van Woerden 1997).

Figure 10 shows the time evolution of of the minimum resolvable mass for each cluster according to 6, which remains much smaller than the local Jeans mass.

4.1 Dark Matter in Cluster Candidates

The candidate labeled as Candidate 0 was the only formed by gas and particles of another species. Figure 13 (a) clearly shows that the predominant mass component is the dark matter of the satellite from where it comes. This dark matter component is not circumstantial, and is an integral part of this candidate during its lifetime. The rest of the candidates are basically cores of gas, without dark matter or disc stars, and even more striking, no new stars formed within the candidate. Without stars, the candidate will never become a cluster, it will remain as a compact core of gas with high density.

5 SUMMARY AND DISCUSSION

In this work, we ran a series of N-body simulations of satellite galaxies undergoing minor mergers with a larger host galaxy, looking for globular cluster-like systems in the tidal stream formed by the tidally stripped material from the satellite. The work was divided in two main parts: The first part was performed to explore the possibility of a completely devoid of gas satellite as progenitor of the cluster-like structures while the second part was dedicated to simulations with isothermal gas in the satellite galaxy.

Then we performed several estimations in the simulations to identify the stream and the possible autogravitating substructures inside it. The approach adopted to identify substructures were the estimation of the phase-space density which will reveal the presence of substructures as density peaks.

The density estimation clearly identifies overdensity regions in which a cluster-like structure could be formed. As a first conclusion we argue that without gas, non long-life substructures could be formed as none of the overdensities show a definite morphology or stability over time. When the gas was included, several clumps appear.

Running with gas physics results are remarkably different. The candidates obtained proved real physical structures that lived for a considerable amount of time and whose orbital evolution leads them to be objects in the surroundings of the galactic disk. The total absence of stars formed within the clumps is mainly due to the thermodynamic setup of the gas as an initially isothermal sphere and probably due to the implementation/parameters of star formation and feedback we used. However, examining the thermodynamic evolution of the clump, the probability of a collapse under real physical conditions seems plausible since quantities as the pressure and the Jeans mass within the candidates could favor cluster formation.

Thus, the exploration of realistic temperatures distributions and another more realistic hydrodynamical parameters of the gas is the path to follow in order to complete the final conclusion of this work; substructures (globular clusters and

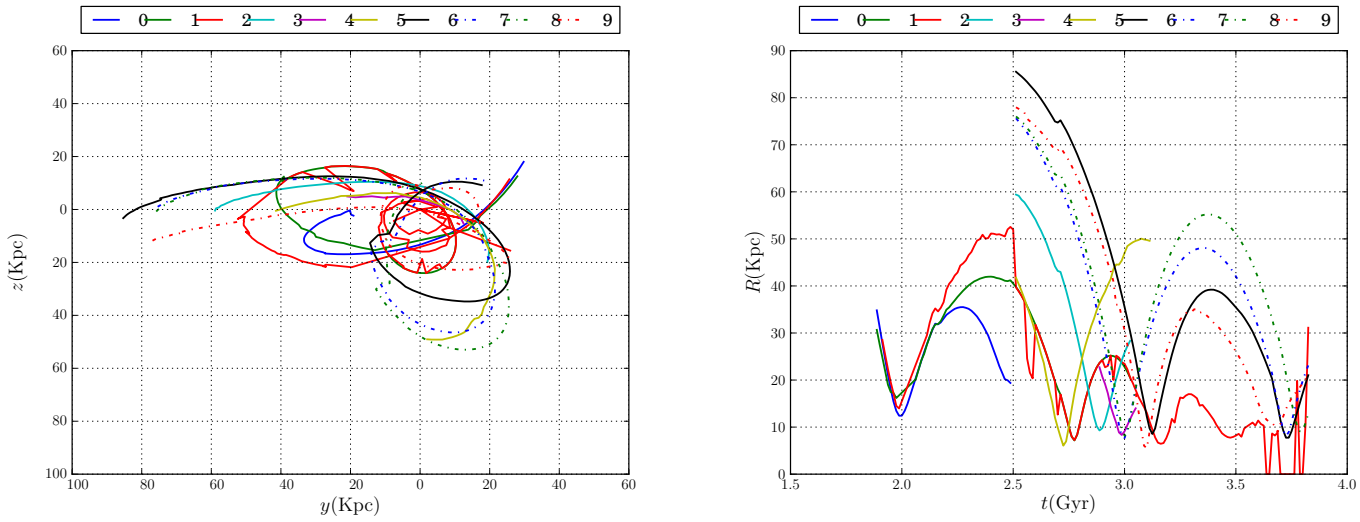

(a) (b)

Figure 11. Orbital structure of the nine candidates identified in GAS3. (a) Projection of the orbits in the yz plane. (b) Magnitude of the galactocentric vector position as a function of time.

high velocity clouds) can be formed in tidal streams of gas rich satellites. The validity and scope of this main conclusion should be tested by running simulations with higher resolutions with the above considerations in the physical modeling of the problem. This is the road map for future work that contributes to improving and supplementing the results presented here.

ACKNOWLEDGMENTS

The authors widely acknowledge the Centro de Investigaciones CIEN ascribed to Facultad de Ciencias Exactas y Naturales from Universidad de Antioquia for their financial support during the last stages of this work. We also are grateful to the Fisica y Astrofísica Computacional group, FACom for facilitates the equipment to perform the complete set of simulations. Finally, we thank Mario Sucerquia for his meaningful comments in the preparation of the paper.

REFERENCES

Ashman, K., & Zepf, S. 1992, ApJ, 384, 50
Bate, M. R., & Burkert, A. 1997, MNRAS, 288, 1060
Bekki, K., & Chiba, M. 2002, ApJ, 556, 245
Bekki, K., & Freeman, K. 2003, MNRAS, 346, L11
Belokurov V., et al., 2006, ApJ, 642, L137
Binney, J. & Tremaine, S. Galactic Dynamics, 2008, Princeton University Press
Binney, J., Nipoti, C. & Fraternali F. 2009, MNRAS, 397, 1804
Blitz L., et al. 1999, ApJ, 514, 818
Carroll, B. W., & Ostlie, D. A, An Introduction to Modern Astrophysics, 2008, Addison-Wesley
Conroy C., et al. 2011, ApJ, 741
Draine, B. T. Physics of the Interstellar and Intergalactic Medium, 2011, Princeton University Press
Elmegreen, B. G., & Efremov, Y. N. 1997, ApJ, 480, 235
Forbes, D. & Bridges, T. 2010, MNRAS, 404, 1203
Forero-Romero, J. E., et al. 2010, MNRAS, 417, 1434
Fraternali F., et al., 2015, MNRAS, 447, L70
Gottloeber, S., Hoffman, Y., & Yepes, G. 2010, arXiv:1005.2687
Harris, W. E. Globular Clusters Systems, 1998, Springer
Harris, W. E. 1999, 10th Canary Islands Winter School of Astrophysics: Globular Clusters, 325
Hernquist L. 1993, MNRAS, 86, 389
Ibata R., et al., 2001, ApJ, 551, 294
Küpper, A. H. W., Lane, R. R.,& Heggie, D. C. 2012, MNRAS, 420, 2700
Li, Y., Law, M., & Klessen, R. 2004, ApJ, 614, L29
Mastropietro, et al. 2005, MNRAS, 363, 509
Mo, H. J., Mao, S., & White, S. D. M. 1998, MNRAS, 295, 319
Moster et al. 2001, ApJ, 710, 903
Norris, M.A. & Kannapan S.J. 2011, MNRAS, 414, 739
Peebles, P.J.E, & Dicke R.H. 1968, ApJ, 154, 891
Sharma S. & Steinmetz, M. 2006, MNRAS, 373, 1293
Springel V. 2005, MNRAS, 364, 1105
Springel V. & White, S. D. M. 1999, MNRAS, 307, 162
Springel V., White, S. D. M. & Hernquist L. 2004, International Astronomical Union Symposium, 421
Springel V. & Hernquist, L. 2002, MNRAS, 333, 649
Torrey, P., et al. 2013, ASP Conference Proceedings, 477, 237
Wakker, B. P., & van Woerden, H. 1997, Annual Review of Astronomy and Astrophysics, 35, 217
Wetzel, A. R. 2011, MNRAS, 412, 49
Zepf, S. & Ashman, K. 1993, MNRAS, 264, 611

This paper has been typeset from a TEX/LATEX file prepared by the author.

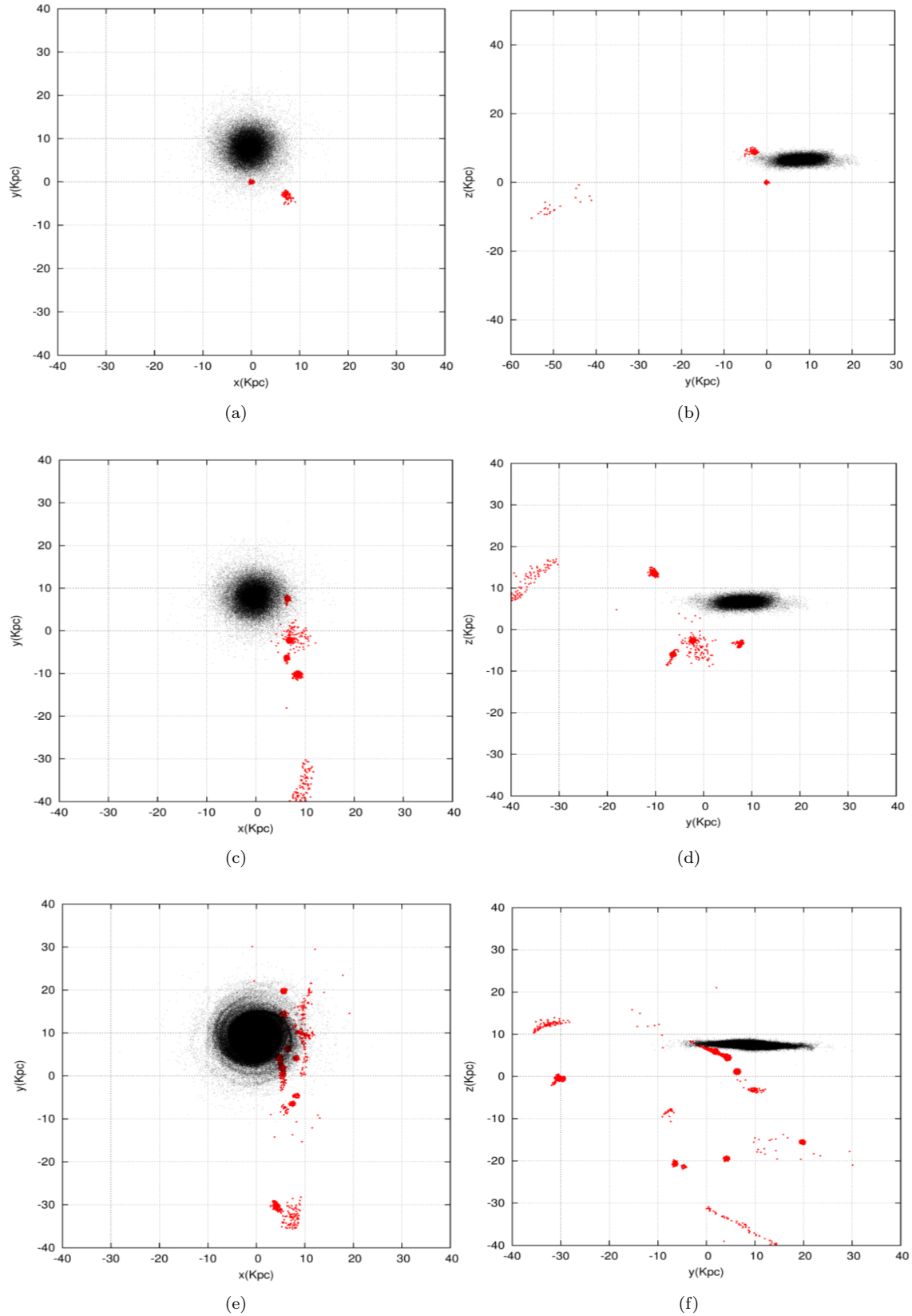

Figure 12. Candidates identified with the algorithm described in this section. The number of clumps increase with increasing resolution. All the plots correspond to 3 Gyr simulation time. (a) Candidates in GAS1 with the disc seen face on. (b) Candidates in GAS1 with the disc seen edge on. (c) Candidates in GAS2 with the disc seen face on. (d) Candidates in GAS2 with the disc seen edge on. (e) Candidates in GAS3 with the disc seen face on. (f) Candidates in GAS3 with the disc seen edge on.

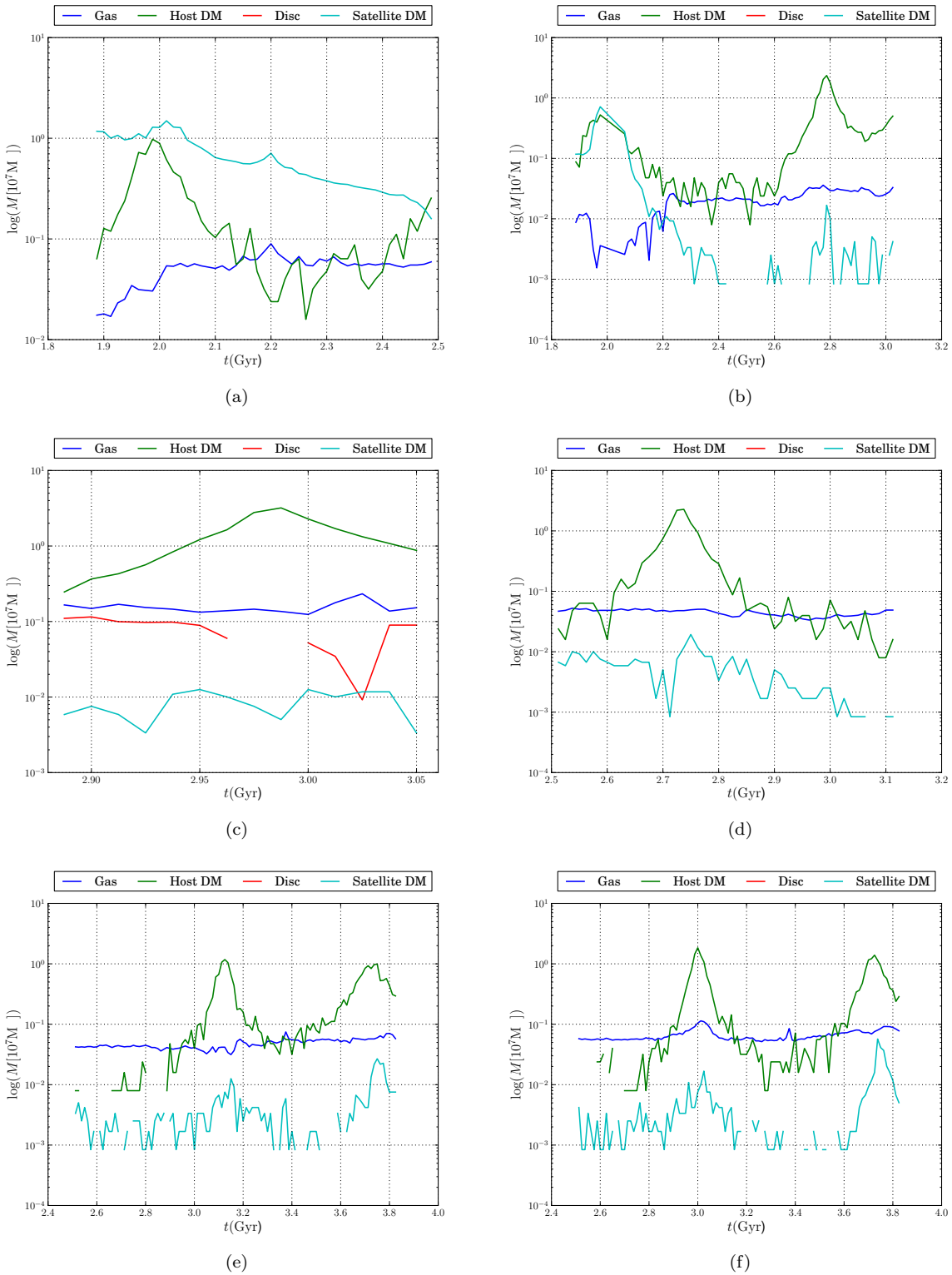

Figure 13. Mass as a function of time for each candidate, segregated by type. The prominent peaks in the plots are due to the pass of the cluster through the central region where the algorithm take into account particles of the dark halo that actually do not belong to the candidate (a) Candidate 0. (b) Candidate 1. (c) Candidate 4. (d) Candidate 5. (e) Candidate 6. (f) Candidate 7.